Journal of Applied Physics ARTICLE scitation.org/journal/jap

Accurate characterization of surface recombination velocities of silicon wafers with differential nonlinear photocarrier radiometry

Cite as: J. Appl. Phys. **131**, 125703 (2022); doi: 10.1063/5.0086624
Submitted: 27 January 2022 · Accepted: 9 March 2022 ·
Published Online: 22 March 2022

Xiaoke Lei, Bincheng Li,[a] Qiming Sun, Jing Wang, and Yafei Wang

AFFILIATIONS

School of Optoelectronic Science and Engineering, University of Electronic Science and Technology of China, Chengdu 610054, China

Note: This paper is part of the Special Topic on Non-Invasive and Non-Destructive Methods and Applications Part I Festschrift.
[a]**Author to whom correspondence should be addressed:** bcli@ uestc.edu.cn

ABSTRACT

The surface recombination velocity (SRV), which reflects the fundamental characteristics of surface defects of semiconductor wafers, is an important parameter in evaluating the quality of surface passivation and electrical performance of surface devices. In conventional photocarrier radiometry (PCR) used for characterizing the electronic transport properties of electronically thick silicon wafers, the rear SRV usually cannot be determined directly due to the relatively low sensitivity of PCR signal to the rear SRV. On the other hand, the determination of front SRV is also very sensitive to the experimental measurement error, especially the measurement error of instrumental frequency response, which is not always easy to be accurately measured in the experiment. In this paper, the front and rear SRVs of silicon wafers are extracted simultaneously with high accuracy by a differential PCR via multi-parameter fitting of the experimental frequency dependences of amplitude ratio and phase difference of PCR signals obtained from the regular measurements and measurements with wafers being flipped respectively to a corresponding differential nonlinear PCR model. The comparison between the front and rear SRVs determined by the conventional and differential PCRs indicates that the differential PCR is highly accurate for the simultaneous determination of the front and rear SRVs of silicon wafers.

I. INTRODUCTION

Industrial solar cells are emerging toward thinner substrates and higher efficiency; meanwhile, the complexity of integrated circuits is increasing, and the number of devices contained in a single chip is increasing sharply so as to continuously reduce costs. The characterization techniques of silicon wafers as the raw material in the fabrication and manufacturing stages play an important role in improving device efficiency and reducing costs in the photovoltaic market and IC industry.[1–7] Photocarrier radiometry (PCR), first proposed by Mandelis *et al.* in 2003,[8] has been developed to be a powerful non-destructive technique for electronic transport characterization of semiconductor wafers. Similar to the well-known infrared photothermal radiometry (PTR), PCR relies on the infrared emission resulting from the radiation recombination of free carriers generated by an intensity-modulated super-bandgap optical source in a semiconductor wafer. PCR is a purely carrier-density-wave detection methodology due to which a near-infrared (NIR) InGaAs detector is used to replace the mid-infrared HgCdTe detector filtering out the thermal component from registered signals. Therefore, all parameters related to the thermal diffusion equation in the PTR theoretical model do not appear in the expression of the PCR signal. As a result, compared to PTR characterization of semiconductor wafers, the number of parameters to be determined via the multi-parameter fitting procedure is reduced in PCR, which results in significantly reduced uncertainty of the fitted electronic transport parameters. Due to the great efforts contributed by Mandelis' team, PCR has achieved a continuous development of theoretical models, improvement of experimental methods, and expansion of applications. At the theory aspect, two-layer,[9] three-layer,[10] and multi-layer[11] linear PCR as well as nonlinear[12] PCR theoretical models were developed; the measurement accuracy of carrier

transport parameters of semiconductor wafers was theoretically analyzed.[13,14] At the experiment aspect, novel PCR techniques such as double-beam PCR[15,16] and time-domain phase-locked PCR[17] were developed. In the application aspect, measurements of carrier transport parameters;[18] detection of impurities and defects;[19,20] monitoring of ion implantation, annealing process,[21] and surface passivation;[22] characterization of ultra-shallow junctions[23] and space charge layer at the Si–SiO_2 interface;[24,25] and investigation of temperature-dependent mobility[26] were reported. In 2010, Mandelis *et al.* further introduced PCR based lock-in carrierography (LIC),[27] which has been applied to carrier effective life imaging[28,29] and polysilicon solar cell material related parameter imaging.[30–32] All these works laid a solid theoretical and technical foundation for the applications of PCR to all-optical measurements and imaging of electronic parameters of semiconductor devices and indicate that PCR has broad industrial application prospects.

In the application of PCR to the measurements of electronic transport parameters of electronically thick c-Si with the carrier bulk lifetime less than 100 μs and the carrier diffusion length $(D^*\tau)^{1/2}$ shorter than the wafer thickness, conventionally the bulk lifetime and diffusion coefficient and the front surface recombination velocity (SRV) are simultaneously determined via multi-parameter fitting of the frequency dependences of PCR amplitude and phase by regular measurements of the semiconductor wafer, while the rear SRV is generally set to a fixed value (for example, to a typical value of 100 m/s for a matte surface).[33] This is largely due to the fact that both the optical absorption length and the carrier diffusion length are shorter than the wafer thickness: (1) the excitation wavelength is usually around 800 nm or even shorter in PCR measurements, and the associated optical absorption length is on the order of or shorter than 10 μm. As a result, the excited carriers are mainly concentrated in the near surface region of the sample under test; and (2) the carrier diffusion length is shorter than the 500-μm wafer thickness widely used in the IC industry, resulting in the relatively small sensitivity of the rear surface recombination velocity to the PCR signal, so which cannot be simultaneously determined with acceptable reliability. Practically, experimental observations have found that SRV increased via sand blowing treatment or rough grinding with carborundum and decreased greatly via fine grinding and surface texturing with appropriate surface passivation mechanism.[4] The surface physical properties and surface states of materials have a great influence on the SRV, which is related to the density of surface recombination center, the capture interface of electrons and holes, and the carrier injection level. The interface is an inherent crystal defect and a relatively effective recombination center and thus the surface of silicon wafer accounts for a considerable proportion in carrier recombination, which requires better surface passivation to reduce the SRV.[34] It has been confirmed that the combination of chemical and field-effect passivation can achieve minimal surface recombination.[35] Any semiconductor device always has its surface. Higher SRV results in a higher recombination rate of the injected carriers on the surface, seriously limiting the performance of the device. Therefore, it is key to obtain an excellent and stable surface in order to minimize the SRV and improve the device performance. The SRV, which reflects the fundamental characteristics of the surface defects, is effective in evaluating the quality of surface passivation and the electrical performance of surface devices.[36]

Up to now, little attention has been paid to the accurate determination of the rear SRV of electronically thick c-Si wafers by PCR. In this paper, the frequency dependences of PCR amplitude and phase were obtained by the regular measurements and measurements with the wafer being flipped (referred to as "flipped measurements" in what follows) of three different silicon wafers (double-polished and single-polished), respectively. The differential PCR data are obtained by normalizing the experimental PCR data from the regular measurements with those from the flipped measurements and then fitted to an appropriate nonlinear PCR theoretical model to determine the electronic transport parameters including both front and rear SRVs via multi-parameter estimation. For comparison, the conventional PCR measurements are also performed through measuring the instrumental frequency response (IFR) and subtracting its influence on the measured PCR signals of silicon wafers. The fitted results with both conventional and differential PCRs are compared and discussed in detail.

II. DIFFERENTIAL PCR THEORY AND SIMULATIONS

Taking the characteristic of the nonlinearity of PCR signal into account, the PCR signal measured from the silicon wafers can be described by[37]

$$S(\omega) = C\int_0^w 2\pi r dr \int_0^L [N_D + 2N(r,z,0)]N(r,z,\omega)dz, \quad (1)$$

where C is a proportionality factor. w is the radius of the effective detection area of the NIR photodetector and L is the thickness of sample. N_D is the doping density, and its value depends on the resistivity of the silicon wafer. $N(r,z,0)$ and $N(r,z,\omega)$ are the dc and ac excess carrier densities, respectively. The basic idea of the differential PCR theory is to use the PCR signal from the flipped measurements to normalize that from the regular measurements so as to obtain the differential amplitude and phase,[38]

$$\begin{cases} A_{\text{diff}} = \dfrac{A_{\text{regular}}(\omega)}{A_{\text{flipped}}(\omega)}, \\ \varphi_{\text{diff}} = \varphi_{\text{regular}}(\omega) - \varphi_{\text{flipped}}(\omega). \end{cases} \quad (2)$$

The numerical simulations are performed to analyze the feasibility of transport parameter determination, especially the simultaneous determination of the rear SRV by PCR. According to the definition of relative sensitivity coefficient,[39] the sensitivity of the PCR signal to the electronic transport parameters is analyzed for the differential and conventional PCRs, respectively, as shown in Fig. 1. A large sensitivity coefficient represents a high sensitivity of PCR signal to that electronic transport parameter, so as to achieve more accurate determination via the multi-parameter fitting. The parameters used in the simulations are $\tau = 23.3\,\mu$s, $D = 16.8\ \text{cm}^2/\text{s}$, $s_1 = 6.54$ m/s, and $s_2 = 15.06$ m/s, respectively. These values are from the experimental data for wafer N_1 presented below.

Figures 1(a) and 1(b) show the frequency dependences of PCR amplitude and phase sensitivity coefficients of transport parameters for the conventional PCR covering the measured frequency range. It is shown that the sensitivity coefficients of amplitude and phase to the transport parameters are small at low frequencies. The bulk

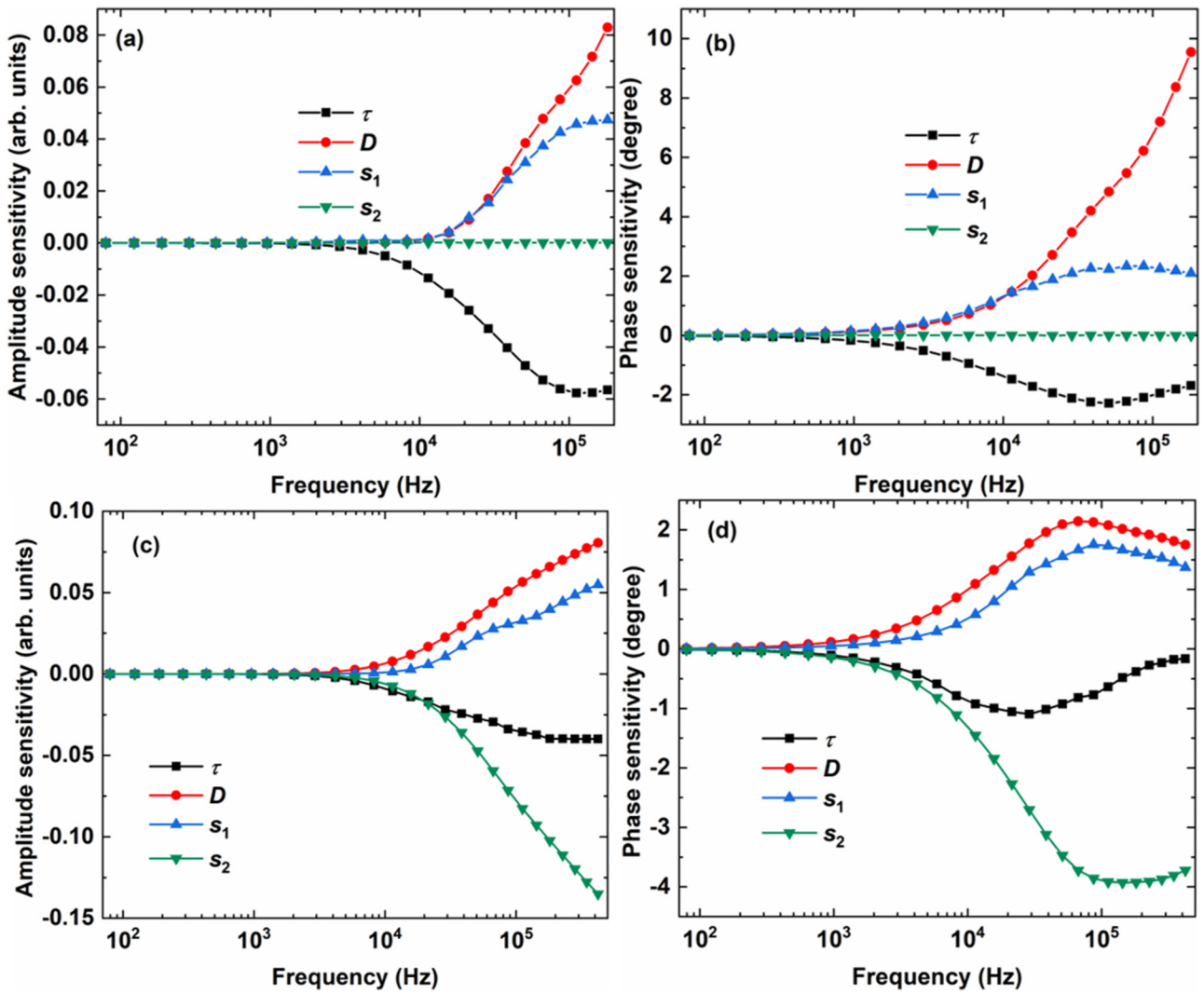

FIG. 1. The sensitivity coefficients of PCR (a) and (c) amplitude and (b) and (d) phase to the four transport parameters as functions of the modulation frequency. (a) and (b) conventional PCR; (c) and (d) differential PCR.

lifetime's sensitivity coefficients for PCR amplitude and phase are negative, and their absolute values first increase with the increasing frequency, reach maxima, and then begin to decline at higher modulation frequencies. The sensitivity coefficients of PCR amplitude and phase to D and s_1 are always positive; the sensitivity coefficients to s_1 increase at first and then decrease at high modulation frequencies, while the sensitivity coefficients to D increase monotonically with the increasing frequency at high modulation frequencies. On the other hand, the sensitivity coefficients to s_2 are small at the whole frequency range, indicating that the PCR amplitude and phase are nearly non-sensitive to the rear SRV. The sensitivity analysis shows that the bulk lifetime, the diffusion coefficient, and the front SRV can be reliably determined by the conventional PCR, while the rear SRV cannot. If the rear SRV needs to be determined, PCR measurements from the rear surface are also needed. It is worthy to mention that at the high-frequency end, PCR amplitude and phase are most sensitive to the diffusion coefficient, so that the diffusion coefficient can be determined via conventional PCR most accurately.

Similarly, the frequency dependences of sensitivity coefficients of PCR amplitude (ratio) and phase (difference) to the transport parameters for the differential PCR are shown in Figs. 1(c) and 1(d), respectively. Again, the sensitivity coefficients are small at low frequencies. The sensitivity coefficients to τ and s_2 are always negative, and the amplitude sensitivity coefficients increase monotonically with the increasing frequency, while the phase sensitivity coefficients increase at first and then decrease at high modulation frequencies. On the other hand, the sensitivity coefficients to D and

s_1 are positive, and their amplitude sensitivity coefficients also increase monotonically with the increasing frequency. Their phase sensitivity coefficients show maxima in the moderate frequency range. It can be seen that at the moderate to high-frequency range, the PCR amplitude and phase are highly sensitive to s_1, s_2, τ, and D, indicating that all the four transport parameters can be reliably determined by the differential PCR. The results also show that PCR amplitude and phase are most sensitive to s_2, indicating that the rear SRV can be determined most accurately via differential PCR.

The above sensitivity analysis shows that the simultaneous determination of τ, D, and s_1 can be fulfilled by the conventional PCR, provided the frequency dependences of PCR amplitude and phase are accurately measured with a high signal-to-noise ratio (SNR). Therefore, in principle, by measuring the frequency dependences of PCR signals from both the front and rear surfaces, τ, D, s_1, and s_2 can be determined separately by the conventional PCR. This is also the basis for the simultaneous determination of τ, D, s_1, and s_2 via the differential PCR. However, the simultaneous determination of the transport parameters via multi-parameter fitting is inherently ill-posed and very sensitive to errors presented in the PCR measurements. For example, relatively large measurement error of IFR, which has significant influence on the accurate measurement of PCR amplitude and phase, is commonly present due to various experimental errors.[40] These measurement errors are present in the measured PCR amplitude and phase in the conventional PCR but are absent in the measured PCR amplitude ratio and phase difference in the differential PCR as the IFR is canceled out by differentiation. Therefore, the reliability of the simultaneous determination of the four transport parameters via the differential PCR is improved as compared to that via the conventional PCR due to the elimination of influence of IFR measurement error on the multi-parameter determination.

III. EXPERIMENTAL AND MATERIALS

The detailed description of the experimental PCR apparatus has been given previously.[38] A semiconductor laser, with a wavelength of 830 nm and excitation power of approximately 45 mW (monitored by a power meter), is periodically modulated by a function generator and then focused onto the sample surface by a focusing lens. In the experiment, a small focusing spot is employed to excite the silicon wafer and then obtain PCR signal with high signal-to-noise ratio (SNR). The radius of tightly focused beam onto the sample surface is approximately 25 μm. The periodic PCR signals are collected through a pair of off-axis paraboloidal mirrors and detected by an InGaAs photodetector whose spectral range of response is from 700 to 1800 nm and the effective detection area radius is approximately 55 μm and then are demodulated by a lock-in amplifier and output the amplitude and phase data. Since the laser with the central wavelength of 830 nm is within the spectral response range of the InGaAs photodetector, it is necessary to use a 1000 nm long pass filter placed in front of the detector to block the excitation laser. In the fitting process, considering the influence of vignetting and defocusing, the effective detection radius of photodetector obtained by fitting the PCR data of a reference sample to the corresponding theoretical model is used instead of the real radius.[41] The absorption coefficient of the crystalline silicon (c-Si) at 830-nm wavelength is set to 6.6×10^4 m^{-1}.[42]

TABLE I. List of silicon wafers used in the experiment and related processing parameters.

Sample	Substrates	Resistivity (Ω cm)	Thickness (μm)
$N_{1,2}$	P-type ⟨111⟩	8–13	525 ± 20
N_3	N-type ⟨100⟩	7–10	525 ± 20

The silicon wafers used in this experiment are divided into two groups by their resistivity values. The detailed processing parameters of the wafers are shown in Table I. Group one (N_1 and N_2) is prepared from a batch of ⟨111⟩ oriented p-type C-Si wafers polished on both surfaces. Only half of the front surface of N_1 wafer is As^+-implanted at 100 keV and the other half are non-implanted by covering a semicircular mask during ion implantation, and then thermally annealed at 1100 °C. N_2 is a wafer without implantation. Group two (N_3) is a wafer of ⟨100⟩ oriented N-type Cz Si wafers with a chemically and mechanically polished front surface and a matte rear surface.

Experimentally, the PCR amplitude and phase as a function of modulation frequency are obtained by the regular and flipped measurements on the non-implanted regions of N_1, N_2, and N_3 wafers, respectively, in order to accurately determine the bulk lifetime (τ), carrier diffusion coefficient (D), and front and rear SRVs (s_1 and s_2). The differential PCR data of N_1 and N_3 are obtained by normalizing the experimental PCR data from the regular measurements with those from the flipped measurements, and then fitting to the differential one-layer nonlinear PCR model to extract the four electronic transport properties (τ, D, s_1, and s_2) via multi-parameter estimation, respectively. Meanwhile, the conventional PCR approach is also used to extract the transport parameters for comparison, in which the instrumental frequency response (IFR) is measured independently and subtracted from the PCR signals.

IV. RESULTS AND DISCUSSION

Experimentally, the measured frequency dependences of PCR amplitude and phase with IFR subtraction are multi-parameter fitted to the conventional one-layer nonlinear PCR model,[37] or the measured frequency dependences of PCR amplitude ratio and phase difference without IFR subtraction are multi-parameter fitted to the corresponding differential nonlinear PCR model to extract the transport parameters. In the conventional PCR, τ, D, and s_1 are set as free variables while s_2 is either set as a free parameter (in this case, s_2 is simultaneously determined together with τ, D, and s_1) or is fixed to a typical value 100 m/s[37] in the multi-parameter fitting to minimize the variance of the deviation between theory and experiment. In these cases, s_1 and s_2 are determined separately by the regular and flipped PCR measurements, respectively. The original PCR signals without IFR subtraction from the regular and flipped measurements are also used to obtain the PCR amplitude ratio and phase difference, which are used for the simultaneous determination of τ, D, s_1, and s_2 via the differential PCR.

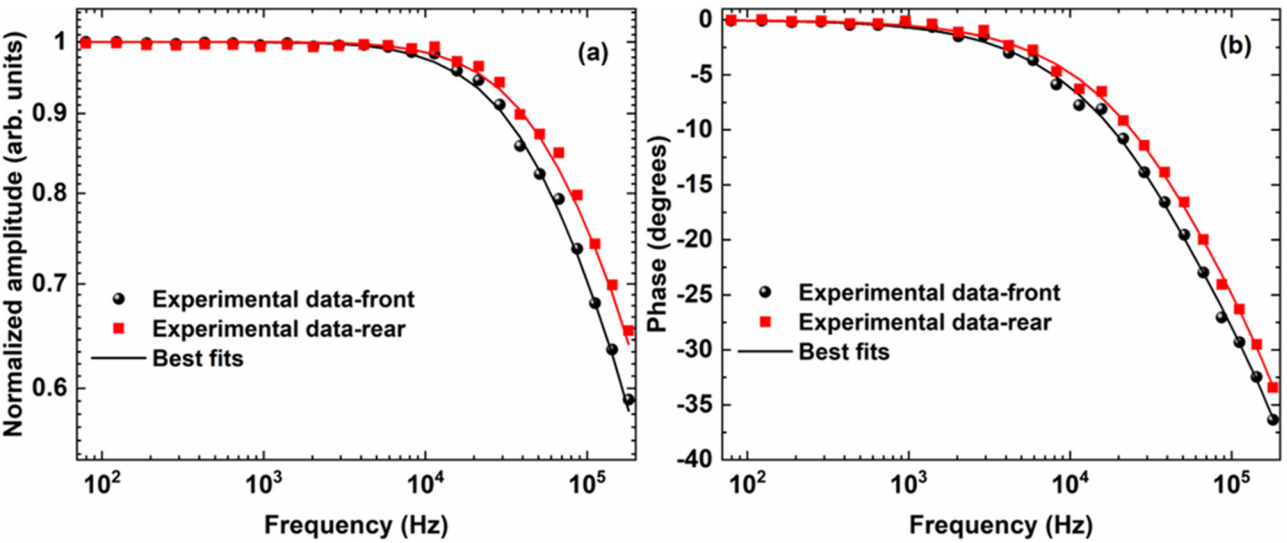

FIG. 2. The frequency dependences of PCR amplitude (a) and phase (b) obtained by the regular and flipped measurements of N_1 wafers. Symbols and solid lines represent the experimental data and the corresponding best fits, respectively.

As examples, Fig. 2 shows the conventional PCR frequency-scanning data of the non-implanted regions of wafer N_1 from the regular and flipped measurements as well as the corresponding theoretical best fits. The PCR amplitude is normalized by the value measured at the lowest frequency, which is 1.02 and 0.95 mV, respectively. Meanwhile, the differential data from the regular and flipped measurements of the non-implanted regions are also utilized to extract the transport parameters by the differential PCR, as shown in Fig. 3. Obviously, good agreements between the experimental data and best-fitted theoretical curves are obtained in both conventional and differential PCRs. Table II summarizes the best-fitted results and variances of the deviation between theory and experiment of the multi-parameter fitting procedures presented in Figs. 2 and 3 for wafer N_1, respectively.

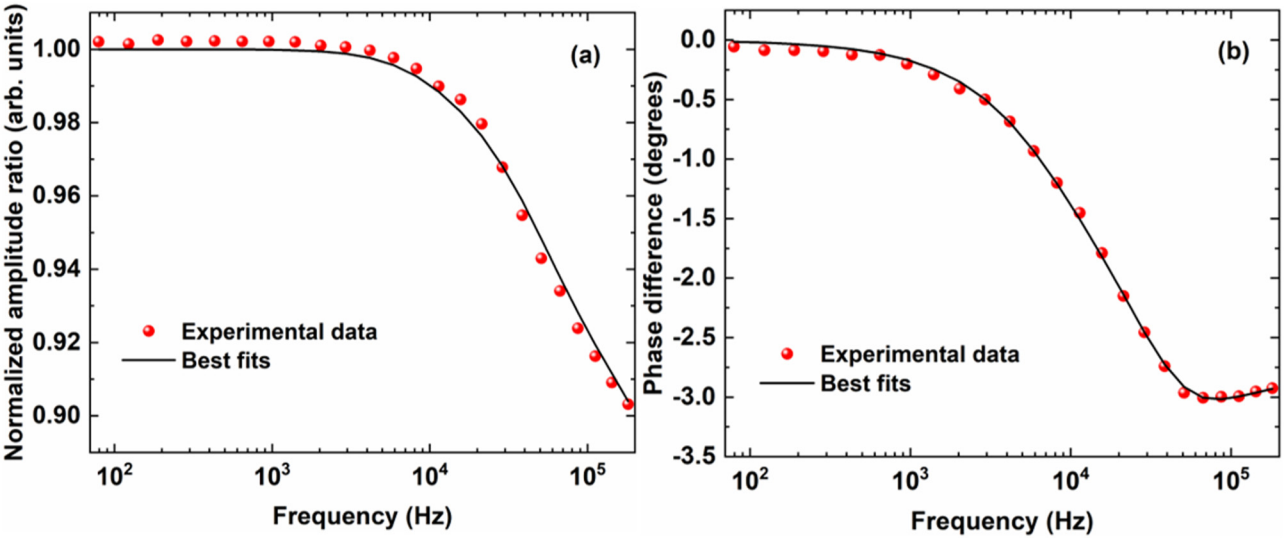

FIG. 3. The frequency dependences of the differential PCR amplitude ratio (a) and phase difference (b) for N_1 wafers. Symbols and solid lines represent the experimental data and the corresponding best fits, respectively.

TABLE II. The transport parameter values determined with the differential and conventional PCRs for wafers N_1 and N_2, respectively. Note: C and D stand for the values obtained from the differential and conventional PCRs. R and F stand for values obtained from the regular and flipped measurements via conventional PCR, respectively. Boldface denotes the relative differences between the fitted parameters determined by two methods.

Sample	Method	τ (μs)	D (cm^2/s)	s_1 (m/s)	s_2 (m/s)	Var (10^{-4})
N_1	Differential	23.3 (±11.4%)	16.8 (±5.64%)	6.54 (±16.1%)	15.1 (±8.9%)	3.41
	Conventional	22.6	17.5	7.23	100 (fixed)	6.51
	(C-D)/C	**3.10%**	**4.10%**	**9.54%**		
	Conventional	21.6 (±11.5%)	17.6 (±9.06%)	6.77 (±16.4%)	5.19 (>50%)	6.49
	Conventional-flipped	21.0	17.5	100 (fixed)	16.5	7.78
	(C-D)/C	**9.87%**	**4.10%**		**8.72%**	
	Conventional-flipped	20.7 (±11.6%)	17.7 (±9.11%)	10.2 (>50%)	15.8 (±16.6%)	7.77
N_2	Conventional	14.9 (±11.6%)	17.7 (±9.66%)	9.17 (s_1=s_2) (±16.8%)		3.99
	Conventional-flipped	13.9 (±11.5%)	18.5 (±9.63%)	8.24 (**s_1=s_2**) (±16.8%)		4.23
	(R-F)/F	**7.19%**	**4.44%**	**11.3%**		

For wafer N_1, the transport parameters determined via the regular and flipped measurements with the conventional PCR under free and fixed s_2 conditions all show excellent consistency. The determined bulk lifetime and diffusion coefficient range from 20.0 to 22.6 μs and from 17.5 to 17.7 cm^2/s, respectively. The front and rear SRV ranges are 7.23–6.77 and 15.8–16.5 m/s, respectively. Only very small changes for τ, D, and s_1 are observed when s_2 changes from fixed to free, indicating that PCR measurements are not sensitive to the rear SRV, and correspondingly the rear SRV cannot be reliably determined via multi-parameter fitting when set as a free parameter. This point is clearly indicated from the fitted results listed in Table II. The results also indicate that the simultaneous determination of τ, D, and s_1 via the conventional PCR is reliable, provided the measured PCR amplitudes and phases are accurate.

On the other hand, the simultaneous determination of τ, D, s_1, and s_2 via the differential PCR is experimentally demonstrated via the results listed in Table II, in which the relative differences between the τ, D, s_1, and s_2 values determined by the conventional PCR (under the fixed rear SRV condition) and differential PCR are present. The relative differences are below 10% for all transport parameters for wafer N_1. Taking into account the uncertainty in the IFR measurement, these relative differences are acceptable.

It is worth mentioning that the differential PCR is applicable only when there is a significant difference between the front and rear SRVs. When there is no or small difference, the amplitude ratio and phase difference are close to unity and zero degree, respectively, approximately independent of the frequency in the whole frequency range. No features in the frequency dependences of PCR amplitude ratio and phase difference can be used to determine the transport parameters. In the case of silicon wafers with (nearly) identical surfaces, the transport parameters can be determined by the conventional PCR with the assumption of equal front and rear SRVs, that is, $s_1 = s_2$ in the multi-parameter fitting. The PCR measurement on N_2 wafer, which has approximately identical treatment process for the front and rear surfaces, is performed and the fitted results are also listed in Table II; the measured and best-fitted frequency dependences of PCR amplitude and phase are presented in Fig. 4. Again, the PCR amplitude is normalized by the value measured at the lowest frequency, 0.92 mV. The agreements are quite good between the results obtained from the regular and flipped PCR measurements. The differences of the fitted τ, D, and $s_1(s_2)$ values are 7.19%, 4.44%, and 11.3%, respectively. These small differences might be caused by a small difference between the defect states of the two surfaces, which can be seen from the variances of the deviation between theory and experiment (3.99×10^{-4} vs 4.23×10^{-4}).

The surface recombination characterization capability of the differential PCR is further investigated by a wafer (N_3) with a polished front surface and a matte rear surface. In this case, the SRV of the matte surface is expected to be much higher than that of the polished surface. Figures 5(a) and 5(b) show the frequency dependences of the PCR amplitude (normalized by the values measured at the lowest frequency, 1.86 and 1.06 mV, respectively) and phase obtained from the regular and flipped measurements and the corresponding theoretical best fits in the conventional PCR. The corresponding PCR amplitude ratio and phase difference as well as the theoretical best fits in the differential PCR are shown in Figs. 5(c) and 5(d), and the fitted results are listed in Table III. From Table III, it is seen that reasonably good agreements between the τ_1, D_1, s_1, and s_2 values determined by the conventional and differential PCRs are obtained. For the regular measurements, the relative differences (with fixed s_2) of the fitted τ_1, D_1, and s_1 values between determined via the two approaches are only 2.78%, 0.52%, and 1.90%, respectively. For the flipped measurements, the corresponding differences (with fixed s_1) of the fitted τ_1, D_1, and s_2 values are 16.6%, 9.17%, and 12.2%, respectively. It is obvious that the SRV values determined by the differential PCR are basically

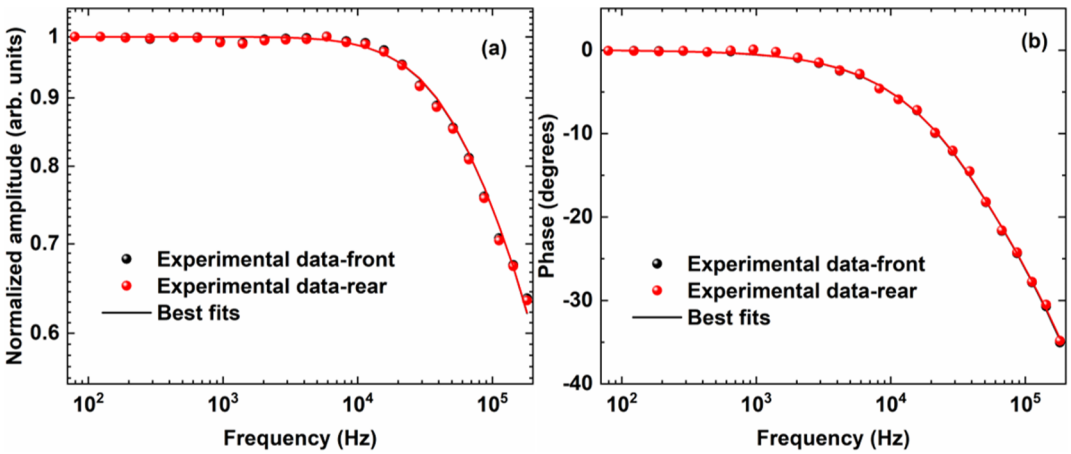

FIG. 4. The frequency dependences of PCR amplitude (a) and phase (b) obtained from the regular and flipped measurements of a double-sided polished N_2 wafer and the corresponding theoretical best fits, respectively.

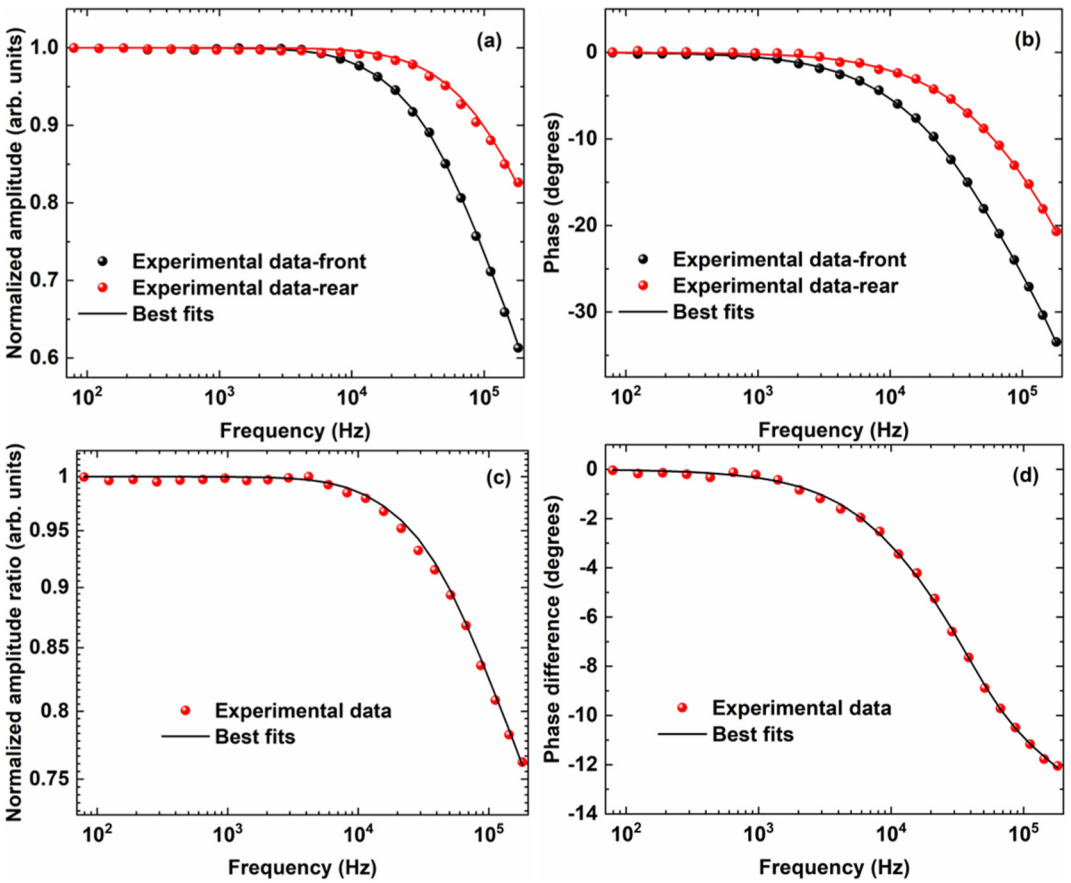

FIG. 5. The frequency dependences of PCR amplitude (a) and phase (b) obtained from the regular and flipped measurements of a single-side polished N_3 wafer in the conventional PCR, and the corresponding (c) amplitude ratio and (d) phase difference in the differential PCR. Symbols and solid lines represent the experimental data and corresponding theoretical best fits, respectively.

TABLE III. The transport parameter values of N_3 wafer with polished front surface and matte rear surface determined via the differential and conventional PCRs. Boldface denotes the relative differences between the fitted parameters determined by two methods.

Approach	τ (μs)	D (cm^2/s)	s_1 (m/s)	s_2 (m/s)	Var (10^{-4})
Differential	21.0 (±12.1%)	20.9 (±9.33%)	9.11 (±17.4%)	123.6 (±9.08%)	3.02
Conventional	20.6	21.01	8.94	100 (fixed)	2.05
(C-D)/C	**2.78%**	**0.52%**	**1.90%**		
Conventional	20.5 (±11.4%)	21.01 (±9.09%)	8.93 (±16.8%)	64.85 (>50%)	2.03
Conventional-flipped	18.01	23.01	100 (fixed)	110.2	3.03
(C-D)/C	**16.6%**	**9.17%**		**12.2%**	
Conventional-flipped					3.03

consistent with that determined by the conventional PCR from regular and flipped measurements separately, which further indicates that the reliability of the differential PCR for the simultaneous determination of the front and rear SRVs. From the SRVs measured with both the conventional and differential PCRs, the typical SRV values of polished surfaces of non-implanted silicon wafers are on the order of several m/s (below 10 m/s) to below 1 m/s, depending on the surface processing procedures, while that of the matte surfaces are in the order of 100 m/s. It is, therefore, quite reasonable to set the rear SRV of a matte surface to 100 m/s in previous publications.

To quantitatively analyze the accuracies of the fitted transport parameters determined by the differential PCR, sensitivity analyses of the determined transport parameters with differential and conventional PCR models for all wafers are performed. The variance of the deviation between theory and experiment is calculated as a function of one parameter while the other three parameters are set as free in the multi-parameter fitting. The ranges of the fitted transport parameters (τ, D, s_1, and s_2) with a 10% change in variance of the deviation between theory and experiment are summarized in Tables II and III. Obviously, the uncertainties of the τ, D, s_1, and s_2 values simultaneously determined via the differential PCR are within the acceptable range. Taking into consideration that in the conventional PCR the determination of the SRVs is subject to the measurement errors of IFR, while in the differential PCR the SRV determination is totally immune to the IFR errors, it is therefore expected that more accurate SRV values are obtained with the differential PCR, especially the rear SRV. The results also indicate that the determinations of D and s_2 are more accurate than that of τ and s_1, as predicted by the sensitivity analysis.

V. CONCLUSIONS

In summary, a differential PCR was proposed to determine simultaneously the front and rear surface recombination velocities of silicon wafers. The major innovation in the differential PCR is that the SRVs s_1 and s_2 together with the bulk lifetime τ and carrier diffusion coefficient D are determined simultaneously without compromising the reliability of the determined τ and D. In addition, the need to measure the IFR in the conventional PCR was totally eliminated in the differential PCR. Good agreements between the transport parameter values determined with the traditional and differential PCRs were achieved, which proved the reliability of the differential PCR for the simultaneous measurements of all four transport parameters including the rear SRV. The experimental results showed that the SRVs of polished surfaces of N-type silicon wafers with 7–10 Ω cm are below 10 m/s and that of matte surfaces are in the order of 100 m/s. The differential PCR is demonstrated to be a useful tool for quality evaluation of surface passivation, which can also offer a potential application prospect for the on-line monitoring of the design and fabrication of silicon-based devices.

ACKNOWLEDGMENTS

The authors thank the financial support by the Natural Science Foundation of China (Grant Nos. 61771103, 61704023, and 61601092).

AUTHOR DECLARATIONS

Conflict of Interest

The authors have no conflicts to disclose.

Ethics Approval

Ethics approval is not required.

DATA AVAILABILITY

The data that support the findings of this study are available from the corresponding author upon reasonable request.

REFERENCES

[1]F.-J. Ma, G. G. Samudra, M. Peters, A. G. Aberle, F. Werner, J. Schmidt, and B. Hoex, J. Appl. Phys. **112**, 054508 (2012).
[2]P. Song, F. Yang, J. Liu, and A. Mandelis, J. Appl. Phys. **128**, 180903 (2020).
[3]S. M. Sze and K. K. Ng, *Physics of Semiconductor Devices* (John Wiley & Sons, 2007).
[4]D. K. Schroder, *Semiconductor Material and Device Characterization*, 3rd ed. (John Wiley & Sons, 2015).
[5]D. K. Schroder, IEEE Trans. Electron Devices **44**, 160 (1997).
[6]J. Giesecke, *Quantitative Recombination and Transport Properties in Silicon From Dynamic Luminescence* (Springer, 2014).

[7]A. Richter, S. W. Glunz, F. Werner, J. Schmidt, and A. Cuevas, Phys. Rev. B **86**, 165202 (2012).
[8]A. Mandelis, J. Batista, and D. Shaughnessy, Phys. Rev. B **67**, 205208 (2003).
[9]C. Wang, A. Mandelis, J. Tolev, B. Burchard, and J. Meijer, J. Appl. Phys. **101**, 123109 (2007).
[10]B. Li, D. Shaughnessy, A. Mandelis, J. Batista, and J. Garcia, J. Appl. Phys. **95**, 7832 (2004).
[11]R. Tai, C. Wang, J. Hu, and A. Mandelis, J. Appl. Phys. **116**, 033706 (2014).
[12]J. Tolev, A. Mandelis, and M. Pawlak, J. Electrochem. Soc. **154**, H983 (2007).
[13]B. Li, D. Shaughnessy, A. Mandelis, J. Batista, and J. Garcia, J. Appl. Phys. **96**, 186 (2004).
[14]B. Li, D. Shaughnessy, and A. Mandelis, J. Appl. Phys. **97**, 023701 (2005).
[15]D. Shaughnessy, A. Mandelis, J. Batista, J. Tolev, and B. Li, Semicond. Sci. Technol. **21**, 320 (2006).
[16]J. Batista, A. Mandelis, D. Shaughnessy, and B. Li, Appl. Phys. Lett. **85**, 1713 (2004).
[17]A. Mandelis, M. Pawlak, C. Wang, I. Delgadillo-Holtfort, and J. Pelzl, J. Appl. Phys. **98**, 123518 (2005).
[18]J. Wang, A. Mandelis, A. Melnikov, S. Hoogland, and E. H. Sargent, J. Phys. Chem. C **117**, 23333 (2013).
[19]D. Shaughnessy and A. Mandelis, J. Electrochem. Soc. **153**, G283 (2006).
[20]J. Xia and A. Mandelis, J. Phys.: Conference Series. **214**, 012107 (2010).
[21]D. Shaughnessy, B. Li, A. Mandelis, and J. Batista, Appl. Phys. Lett. **84**, 5219 (2004).
[22]A. Melnikov, B. Halliop, A. Mandelis, and N. P. Kherani, Thin Solid Films **520**, 5309 (2012).
[23]J. A. Garcia, X. Guo, A. Mandelis, D. Shaughnessy, L. Nicolaides, and A. Salnik, Eur. Phys. J. Spec. Top. **153**, 287 (2008).
[24]A. Mandelis, J. Batista, J. Gibkes, M. Pawlak, and J. Pelzl, J. Appl. Phys. **97**, 083507 (2005).
[25]A. Melnikov, A. Mandelis, B. Halliop, and N. P. Kherani, J. Appl. Phys. **114**, 244506 (2013).
[26]J. Batista, A. Mandelis, and D. Shaughnessy, Appl. Phys. Lett. **82**, 4077 (2003).
[27]A. Melnikov, A. Mandelis, J. Tolev, P. Chen, and S. Huq, J. Appl. Phys. **107**, 114513 (2010).
[28]Q. Sun, A. Melnikov, and A. Mandelis, Appl. Phys. Lett. **101**, 242107 (2012).
[29]Q. Sun, A. Melnikov, and A. Mandelis, in *40th IEEE Photovoltaic Specialists Conference*, *Denver, CO* (IEEE, 2014), p. 1860.
[30]A. Mandelis, Yu. Zhang, and A. Melnikov, J. Appl. Phys. **112**, 054505 (2012).
[31]J. Liu, A. Melnikov, and A. Mandelis, J. Appl. Phys. **114**, 104509 (2013).
[32]J. Liu, A. Melnikov, and A. Mandelis, Phys. Status Solidi A **210**, 2135 (2013).
[33]A. A. Istratov, H. Hieslmair, and E. R. Weber, Appl. Phys. A **70**, 489 (2000).
[34]R. S. Bonilla, F. Woodcock, and P. R. Wilshaw, J. Appl. Phys. **116**, 054102 (2014).
[35]A. G. Aberle, Prog. Photovolt. Res. Appl. **8**, 473 (2000).
[36]B. Hoex, S. B. S. Heil, E. Langereis, M. C. M. van de Sanden, and W. M. M. Kessels, Appl. Phys. Lett. **89**, 042112 (2006).
[37]Q. Wang and B. C. Li, J. Appl. Phys. **118**, 215707 (2015).
[38]Q. Huang and B. Li, Rev. Sci. Instrum. **82**, 043104 (2011).
[39]X. R. Zhang, B. C. Li, and X. M. Liu, J. Appl. Phys. **104**, 103705 (2008).
[40]X. K. Lei, B. C. Li, Q. M. Sun, J. Wang, C. M. Gao, and Y. F. Wang, Infrared Phys. Technol. **111**, 103533 (2020).
[41]B. Li, D. Shaughnessy, and A. Mandelis, Rev. Sci. Instrum. **76**, 063703 (2005).
[42]E. D. Palik, *Handbook of Optical Constants of Solids* (Academic Press, 1998).